Chromatin Remodeling Due to Transient-Link-and-Pass Activity Enhances Subnuclear Dynamics

Rakesh Das,[1,*] Takahiro Sakaue,[2] G. V. Shivashankar,[3,4] Jacques Prost,[1,5,†] and Tetsuya Hiraiwa[1,6,‡]
[1]Mechanobiology Institute, National University of Singapore, Singapore 117411, Singapore
[2]Department of Physical Sciences, Aoyama Gakuin University, Kanagawa 252-5258, Japan
[3]Department of Health Sciences and Technology (D-HEST), ETH Zurich, Villigen 8092, Switzerland
[4]Division of Biology and Chemistry, Paul Scherrer Institute, Villigen 5232, Switzerland
[5]Laboratoire Physico Chimie Curie, Institut Curie, Paris Science et Lettres Research University, 75005 Paris, France
[6]Institute of Physics, Academia Sinica, Taipei City 115201, Taiwan

(Received 7 June 2023; accepted 2 January 2024; published 31 January 2024)

Spatiotemporal coordination of chromatin and subnuclear compartments is crucial for cells. Numerous enzymes act inside nucleus—some of those transiently link and pass two chromatin segments. Here, we study how such an active perturbation affects fluctuating dynamics of an inclusion in the chromatic medium. Using numerical simulations and a versatile effective model, we categorize inclusion dynamics into three distinct modes. The transient-link-and-pass activity speeds up inclusion dynamics by affecting a slow mode related to chromatin remodeling, viz., size and shape of the chromatin meshes.

DOI: 10.1103/PhysRevLett.132.058401

Genetic information of a eukaryotic cell is stored in its chromatin, a ∼2 m long polymeric entity comprising DNA and histone proteins, which is packed inside the nucleus typically of size 7–10 μm. In addition to the chromatin, the nucleus contains a diverse variety of subnuclear compartments (SNCs) like nucleoli, speckles, Cajal bodies, promyelocytic leukemia bodies, transcription factories, etc., ranging from ∼50 nm to 1 μm in sizes, all dispersed in a viscous fluid medium called nucleoplasm [1–5]. A spatiotemporal coordination among these SNCs and the chromatin is necessary for the healthy functionality of the cell [2–8], the lack of which correlates with several diseases [9,10].

Recent studies have attributed such spatiotemporal coordination of SNCs and chromatin to the mechanical state of chromatin. Reference [11] shows that coalescence kinetics of inert liquid droplets dispersed inside a nucleus depends on their dynamics dictated by the mechanics of the chromatic environment, whereas Ref. [12] shows how the number, size, and localization of such subnuclear condensates are dictated by chromatin mechanics. We found in our earlier study [13] that transient-link-and-pass activity (TLPA) associated with ATP-dependent actions of some classes of enzymes, like Topoisomerase-II [14–17], can affect the microphase-separation structure of heterochromatin or euchromatin—this enables us to speculate that, even in a homogeneous medium of chromatin, e.g., even when looking into only the euchromatin part, enzymatic activities could affect local mechanical states of chromatin. Such change in the local mechanical state of chromatin could eventually affect dynamics of finite-size inclusions such as SNCs. Indeed, it is known that the dynamics of the chromatin and other SNCs are usually ATP-dependent [18–25], and ATP-dependent remodeling of the chromatic environment is recognized as one of the mechanisms for this dependency [24–26]. Despite its possible relevance for biological functions, up to the present, no studies have clarified if an active perturbation like TLPA actually plays a role in inclusion dynamics and what kind of chromatic remodeling can contribute to it.

In this Letter, we study the effects of an active perturbation on the chromatic medium and fluctuating dynamics of an inclusion, and investigate the underlying physical mechanisms. For this purpose, we consider a single polymer chain subjected to TLPA as a chromatin model, and a finite-size bead disconnected from the polymer chain as an inclusion, inside a spherical cavity [Fig. 1(a)]. To implement TLPA, we follow our earlier work in which a model enzymatic activity was constructed imagining Topoisomerase-II [13]. Through numerical simulations of our model, we first show that TLPA indeed affects the inclusion dynamics. After that, we investigate what kind of chromatin remodeling is associated with this effect. Finally, we construct an effective model that is a fluctuating free particle model but keeps the essence to reproduce the TLPA dependency of the inclusion dynamics observed in our simulation. Using the effective model, we identify the three major dynamical modes in the system.

So far, experimentally observed features of SNC dynamics have been explained quantitatively by a combination of its diffusion within the chromatic-interspace region, plus the translocation of that region due to chromatin diffusion (which we refer to as fast and normal diffusive modes, respectively, later in the text) [25]. However, in general,

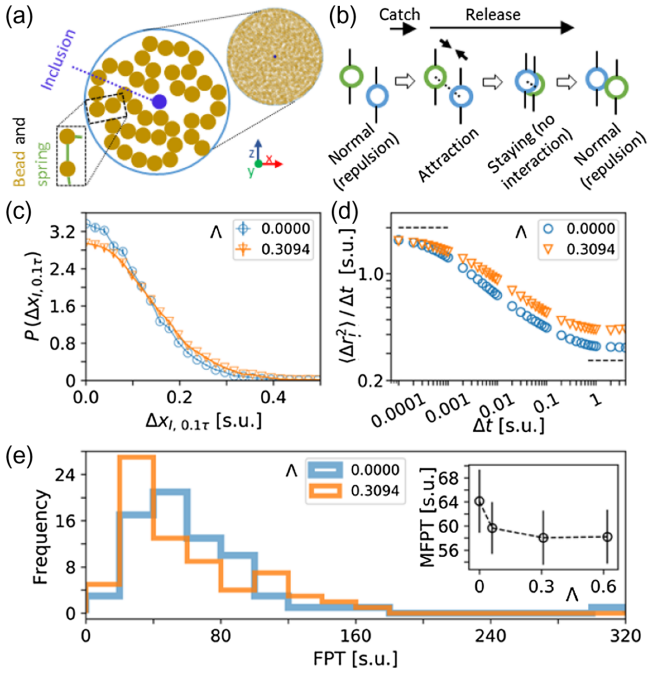

FIG. 1. (a) Bead-and-spring homopolymer model of chromatin packed inside a spherical cavity together with an inclusion at the center; a schematic and a typical simulation snapshot are shown. (b) Catch-and-release mechanism of Topoisomerase-II's enzymatic activity. There is no steric repulsion between the pair of the beads when bound to the enzyme. (c) Mean ± SEM of $\Delta x_{I,0.1\tau}$ distribution are shown. Only the positive half is shown for better representation. (d) MSDs of the inclusion are shown for several Λ. Dashed lines are to guide the early-time and the late-time diffusion. (e) Main: FPT distribution of the inclusion to the radius $R = 5\ell$ of the cavity starting from $R = 0$ ($n = 71$). Inset: Λ dependency of the mean ± SEM of FPT. SFig. 1 supplements Figs. 1(c)–1(e) with curves for four Λ values.

chromatic interspace itself can remodel, i.e., its size and shape can change, and thus affect SNC dynamics [24]. In particular, mechanical actions of enzymes like TLPA may directly drive such chromatin remodeling. The effective model proposed here indeed demonstrates the relevance of a slow dynamical mode linked to chromatin remodeling for the TLPA-dependent inclusion dynamics.

Model.—We develop a self-avoiding linear homopolymer model for the chromatin confined within a spherical cavity of diameter D [Fig. 1(a)]. The homopolymer comprises N soft-core beads of diameter d_B consecutively connected by finitely extensible nonlinear elastic springs. A hard-core spherical inclusion of diameter d_I is placed at the center of the cavity. This inclusion experiences steric forces due to the surrounding polymer.

The dynamics of the positions of the beads ($\boldsymbol{x}_B$) and the inclusion ($\boldsymbol{x}_I$) are approximated by Brownian dynamics; see Supplemental Material [27] and Ref. [13] for details. Stokes' relation has been assumed to mimic the frictional drag due to implicitly considered nucleoplasm. Setting the thermal energy and the nucleoplasmic viscosity to unity, and $D = 12\ell$, we obtain the simulation units (s.u.) of length (ℓ), time (τ), and energy (e).

TLPA is implemented in the following sequential manner, which we call catch-and-release mechanism. In the normal state, any pair of spatially proximal beads experiences steric repulsion due to each other (self-avoidance potential $h_{\rm vex} > 0$; see Supplemental Material [27]). The enzyme can catch that pair of beads with a Poisson rate $\lambda_{\rm ra}$ [Fig. 1(b)], and upon that, the beads attract each other ($h_{\rm vex} < 0$). Next, the attraction between those two beads is turned off with another Poisson rate $\lambda_{\rm an}$, and the beads stay there for a while without any steric interaction among themselves ($h_{\rm vex} = 0$). Eventually, the enzyme unbinds from the beads with a Poisson rate $\lambda_{\rm nr}$, and the beads return to their normal state with steric repulsion between themselves. Therefore, in our model, enzymatic activity is realized by the following sequence of Poisson transitions of the steric interaction between a pair of proximal beads: $\text{state}(h_{\rm vex} > 0) \xrightarrow{\lambda_{\rm ra}} \text{state}(h_{\rm vex} < 0) \xrightarrow{\lambda_{\rm an}} \text{state}(h_{\rm vex} = 0) \xrightarrow{\lambda_{\rm nr}} \text{state}(h_{\rm vex} > 0)$. These steps allow the beads to pass across each other stochastically and thereby perturb the medium [13].

We parametrize TLPA as $\Lambda = \lambda_{\rm ra}(1/\lambda_{\rm an} + 1/\lambda_{\rm nr})$, which can be tuned in experiments by controlling ATP concentration [33]. We choose $\lambda_{\rm an} = 16.7\tau^{-1}$ and $\lambda_{\rm nr} = 500\tau^{-1}$ and tune $\lambda_{\rm ra}$ to control the activity. For a given Λ, we integrate the equations of motion of $\boldsymbol{x}_B$ and $\boldsymbol{x}_I$ using Euler discretization method, and thereby we simulate the dynamics of the polymer and the inclusion. This choice of the rates sets a typical timescale $t_{\rm TLPA} = (1/\lambda_{\rm an} + 1/\lambda_{\rm nr}) \simeq 0.062\tau$ for which an enzyme catches a pair of beads. We have checked that by this timescale, a bead typically moves over only $\mathcal{O}(d_B)$.

Each realization of the simulation starts from a steady-state configuration of a self-avoiding polymer packed inside the cavity together with the inclusion at the center of the cavity. The polymer and the inclusion follow the Brownian dynamics as described above. We note that the inclusion eventually touches the cavity boundary; so, we simulate our active polymer model (APM) until the inclusion touches the cavity boundary for the first time. The results reported below are obtained from n number of independent realizations. (See Supplemental Material [27] for further details.)

Inclusion dynamics.—We first investigate how inclusion dynamics is affected by TLPA by looking into its (i) one-dimensional displacement over a given time duration, (ii) mean-square-displacement (MSD), and (iii) first passage time (FPT) in the chromatic medium. Here, we consider an inclusion of size comparable to that of the bead size ($d_I = 0.40\ell$, $d_B \simeq 0.43\ell$).

First, we compare the distribution $P(\Delta x_{I,0.1\tau})$ of one-dimensional displacement of the inclusion over a time duration $\Delta t = 0.1\tau > t_{\rm TLPA}$ for several Λ [Fig. 1(c)]. We note that $P(\Delta x_{I,0.1\tau})$ follows a Gaussian distribution and

widens with Λ. The distributions appeared to be symmetric around zero, although with some fluctuations. However, we did not find any drift in the inclusion dynamics (SFig. 2).

Next, we calculate MSD of the inclusion as $\langle \Delta r_I^2(\Delta t)\rangle = \langle |\boldsymbol{x}_I(t_0+\Delta t) - \boldsymbol{x}_I(t_0)|^2\rangle$, where $\langle\cdot\rangle$ represents average over several t_0 and realizations. We note (A) a short early-time diffusive regime, (B) an intermediate subdiffusive regime, and (C) a late-time diffusive regime. Following this regime (C), we note a significant slowing down of the inclusion dynamics (data not shown). We check that by this time, the inclusion reaches close to the cavity boundary, and although the inclusion does not interact with the boundary, its dynamics is indirectly affected by the polymeric density at that locality that differs from the bulk region. The effect of TLPA at that locality has a different physics than that in the bulk region, and therefore, it will be discussed in the future. In this Letter, we focus on the bulk region (up to radius $R = 5\ell$ instead of the whole cavity of radius $R = 6\ell$). We show the regimes (A)–(C) of the inclusion MSD in Fig. 1(d). Note that the crossover time from the early-time regime to the intermediate regime increases with Λ.

FPT represents the time that the inclusion takes to reach $R = 5\ell$ for the first time starting its dynamics from $R = 0$ at time $t = 0$. We prepare a histogram of the FPTs noted for several realizations of simulation and note that Λ affects it (Fig. 1(e) main). Starting from a high value of the mean FPT (MFPT) for $\Lambda = 0$, it decreases monotonically up to a moderate Λ [Fig. 1(e) inset]. Taking the displacement distributions, MSDs, and the FPT data together, we conclude that TLPA enhances the inclusion dynamics.

Chromatic environment.—The enhancement of the inclusion dynamics should be attributed to some change in the chromatic environment due to TLPA. To investigate it in detail, we compare the polymeric configurations with and without TLPA. We note that the polymeric environment becomes more heterogeneous with Λ [Fig. 2(a), Supplemental Videos). The mean density of the beads, n_B, increases with Λ (SFig. 3). Along with that, the spatiotemporal fluctuation in n_B, as manifested by its standard deviation σ_B, also increases with Λ [Fig. 2(b)], suggesting an increase in heterogeneity of chromatin medium with TLPA.

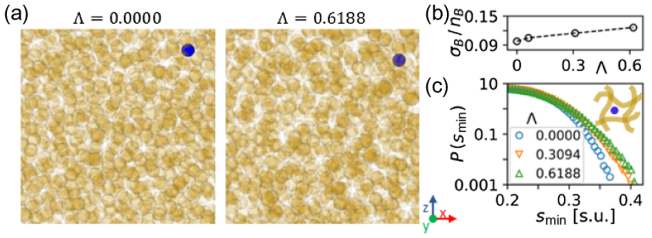

FIG. 2. (a) Cropped slices (6×6 in s.u.) of typical simulation snapshots are shown for $\Lambda = 0$ (left) and 0.6188 (right). (b) Fluctuation σ_B in local density n_B of beads increases with Λ ($n = 71$). (c) Main: distribution of the separation between an arbitrary point and its nearest polymeric bead. Λ-dependent increase in the largest $s_{\min}$ with $P(s_{\min}) > 0$ indicates increase in chromatic mesh size. Data for $s_{\min} < 0.2$ are not shown as the arbitrary points fall on the beads ($d_B \simeq 0.43$ s.u.) in that range. Inset: schematic of the inclusion inside a chromatic mesh.

To further elaborate on this observed heterogeneity, we calculate the separation $s_{\min}$ of any arbitrary point in the bulk region of the cavity to its nearest bead and prepare its distribution $P(s_{\min})$. As a corollary to the increasing heterogeneity in chromatic environment, we note that the tail of $P(s_{\min})$ becomes heavier with Λ [Fig. 2(c)]. The largest $s_{\min}(\Lambda)$ with nonzero $P(s_{\min})$ minus $d_B/2$ could be interpreted as half of the mesh size in the corresponding chromatic environment. It is evident from Fig. 2(c) (main) that the typical mesh size increases with Λ. Considering the $\langle \Delta r_I^2\rangle$ data, it is straightforward to understand that the inclusion performs early-time diffusion until it feels the mechanical hindrance due to its chromatic neighborhood beyond which it shows subdiffusion [Fig. 2(c) schematic].

Effective model.—Next, we develop an integrative understanding of chromatic environment-mediated effect of TLPA on inclusion dynamics. We hypothesize that inclusion dynamics in our APM could be mimicked by its Brownian dynamics with colored noise defined over a coarse-grained timescale δt. Therefore, we conceive a coarse-grained effective model—the inclusion is considered alone, and its dynamics is given by

$$\partial_t \boldsymbol{x}_I = v_{\mathrm{EM}} \boldsymbol{\zeta}_{\mathrm{EM}}, \tag{1}$$

where the right-hand side is an effective noise whose characteristics can be defined from the Λ-dependent behavior of the displacement vector $\Delta \boldsymbol{x}_{I,\delta t}$ defined over δt. More specifically, $v_{\mathrm{EM}}^2 = \langle |\Delta \boldsymbol{x}_{I,\delta t}|^2\rangle/(\delta t)^2$, and $\boldsymbol{\zeta}_{\mathrm{EM}}$ is a Gaussian noise with zero mean and autocorrelation $\langle \boldsymbol{\zeta}_{\mathrm{EM}}(0) \cdot \boldsymbol{\zeta}_{\mathrm{EM}}(\Delta t)\rangle = C_{\Delta \boldsymbol{x}_{I,\delta t}}(\Delta t) = \langle \sum_{t_0} [\Delta \boldsymbol{x}_{I,\delta t}(t_0) \cdot \Delta \boldsymbol{x}_{I,\delta t}(t_0 + \Delta t)] / \sum_{t_0} |\Delta \boldsymbol{x}_{I,\delta t}(t_0)|^2\rangle$ ($\langle\cdot\rangle$ indicating average over several realizations). Hereafter, we consider $\delta t = 0.003\tau$ over which the inclusion dynamics should be affected by the dynamics of its chromatic neighborhood [Fig. 1(d); also see SFig. 4).

We obtain $C_{\Delta \boldsymbol{x}_{I,\delta t}}(\Delta t)$ from our simulation data for several Λ. A negative autocorrelation is noted for $\Delta t \geq \delta t$ [Fig. 3(a) inset] as expected for our current model system—(visco-)elasticity of polymeric medium surrounding the inclusion may tend to reverse the direction of inclusion motion [34]. The negative part of the autocorrelation shows good fit to double exponential function [Fig. 3(a) main]. Therefore, we write $C_{\Delta \boldsymbol{x}_{I,\delta t}}(\Delta t) = A\delta(\Delta t) - g(\Delta t)$ with $g(\Delta t) = a_f e^{-\Delta t/t_f} + a_s e^{-\Delta t/t_s}$, where the fitting parameters $a_{f,s}$ and $t_{f,s}$ depend on Λ. The parameter A takes care of the autocorrelation for $\Delta t < \delta t$.

Using the effective model, we analytically obtain MSD of the inclusion as

$$\langle \Delta r_{I,\mathrm{EM}}^2(\Delta t)\rangle = \sum_{m \equiv f,s} 2D_m t_m \left(1 - e^{-\frac{\Delta t}{t_m}}\right) + 2D_n \Delta t, \tag{2}$$

where $D_{f,s} = v_{\mathrm{EM}}^2 a_{f,s} t_{f,s}$ and $D_n = v_{\mathrm{EM}}^2 (A/2 - a_f t_f - a_s t_s)$ (Supplemental Material [27]). Treating A as a Λ-dependent fitting parameter, we find good agreement between $\langle \Delta r_I^2 \rangle$ and $\langle \Delta r_{I,\mathrm{EM}}^2 \rangle$ (SFigs. 5 and 6). Thus, our simulation results are successfully reproduced by the effective model, where the chromatic environment-mediated effect of TLPA on the inclusion dynamics is captured by the Λ dependency in the features of the coarse-grained noise. Below we show that the construction of the effective model allows us to unveil the physical mechanism how TLPA affects the inclusion dynamics.

We identify the MSD terms corresponding to $m \equiv f$, s with that obtained for a particle subjected to a harmonic potential following an overdamped Langevin equation (Supplemental Material [27]). This gives us a diffusivity D_m and a characteristic time t_m for the mode m. Thus, the inclusion dynamics can be understood as that dictated by a fast (f) and a slow (s) mode (with $t_f \sim 0.002\tau$ and $t_s \sim 0.02\tau$), plus a normal (n) diffusive mode. The n mode originates from the delta-correlated forces that the inclusion feels due to the thermal noise, plus the polymeric neighborhood coarse-grained over δt. The origin of the fast and slow modes must underlie in the fluctuation in the potential that the inclusion feels due to its polymeric neighborhood; we indeed found that the fluctuation in the number of the beads interacting with the inclusion has the characteristic timescale comparable to that of the fast mode, whereas remodeling of the polymeric mesh around the inclusion has the timescale comparable with the slow mode (SFig. 7, Supplemental Material [27]). One can visualize the corresponding scenario as follows: let us consider a polymeric mesh comprising some number of beads around the inclusion. At the scale of $\sim 0.002\tau$, that number fluctuates because of the individual bead's thermal fluctuation (see SFig. 8 for bead's MSD), and therefore the potential fluctuates. This leads to the fast mode contribution to inclusion dynamics. However, at a longer timescale $\sim 0.02\tau$, the size and shape of the mesh are reconfigured leading to another source of the potential fluctuation. This dictates the slow mode contribution to the inclusion dynamics.

Lastly, we investigate which mode mainly contributes to the speeding of the inclusion dynamics with TLPA. Figure 3(b) (main) plots the parts of MSD, $\langle \Delta r_{I,\mathrm{EM}}^2 \rangle$, separately derived from all the three modes. We find that the Λ dependency in MSD at the intermediate timescale ($\sim 0.001 < \Delta t < \sim 0.02$) is dominated by that of the s mode. We note a significant increase in D_s with Λ [Fig. 3(b) top inset; SFig. 9). These results suggest that significant initial speeding up of the inclusion dynamics [around $\Delta t = 0.001$ in Fig. 1(d)] is induced through s mode, which is associated with the chromatin remodeling. In conclusion, TLPA-assisted remodeling of the chromatic neighborhood plays a major role in enhancing the inclusion dynamics. (See Supplemental Material [27] for discussion on Λ dependency of all three diffusivities).

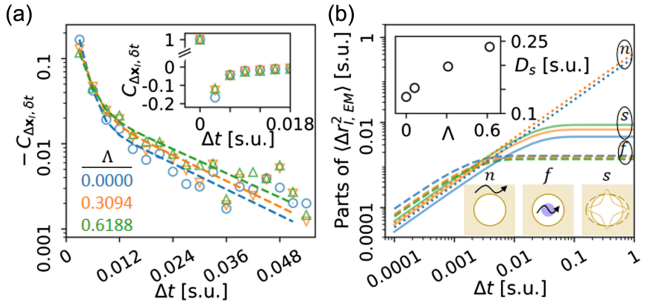

FIG. 3. (a) Autocorrelation $C_{\Delta \boldsymbol{x}_{I,\delta t}}(\Delta t)$ of the inclusion's displacement vector $\Delta \boldsymbol{x}_{I,\delta t}$ over $\delta t = 0.003\tau$ for several Λ (symbols). Main: semilog plot to focus on the negative part of $C_{\Delta \boldsymbol{x}_{I,\delta t}}$. Inset: linear plot. Dashed lines are fits to $-C_{\Delta \boldsymbol{x}_{I,\delta t}}(\Delta t > 0)$ with the double exponential function, $g(\Delta t)$. (b) Main: parts of $\langle \Delta r_{I,\mathrm{EM}}^2 \rangle$ corresponding to the three dynamical modes (n, f, and s) for several Λ [see Fig. 3(a) for legends]. Top inset: Diffusivity corresponding to s mode increases with Λ. Bottom inset: schematic of each mode. Golden: chromatin media. Blue: inclusion.

Discussion.—In summary, through numerical simulations of APM and construction and analysis of the effective model, we investigated the effect of enzymatic action-induced TLPA on the inclusion dynamics in the chromatin environment. We showed that the inclusion dynamics in this complex medium comprises three modes: a fast mode dynamics within the local polymeric mesh, a slow mode dynamics associated with the polymeric reconfiguration, and a normal diffusive mode. TLPA speeds up the inclusion dynamics by significantly facilitating chromatin remodeling. This finding is in line with Ref. [24] where the authors emphasized the importance of ATP-dependent chromatin remodeling to explain their experimental observation. In Ref. [25], as briefly mentioned above, an effective model combining the fast and the normal diffusive modes has been proposed to explain the inclusion dynamics. Our results further showed the necessity of the slow mode associated with chromatin remodeling to fully understand the inclusion dynamics in active chromatic media [schematics in Fig. 3(b) bottom inset]. In Ref. [26], significant slowing down of transcription compartments' dynamics upon depression of temperature from 37 °C to 25 °C has been attributed to temperature-dependent active processes. The chromatin-remodeling-associated dynamical mode reported here can be responsible for that experimental observation. Our current study also implicates how a global active perturbation may regulate site-specific target searching of SNCs by enhancing their encounter frequency [8,35,36]. Furthermore, as Topoisomerase-II activity is known to correlate with cell cycle [37], aging [38], and nucleoplasmic ATP content [39], our study may elucidate such cell state-dependent subnuclear dynamics.

Despite apparent similarity in the inclusion dynamics for various model scenarios in terms of a coarse-grained

TABLE I. Mean ± SEM propagated from both the MFPTs.

d_I	0.2ℓ	0.4ℓ	1.2ℓ
$\mathrm{MFPT}_{\Lambda=0.3094}/\mathrm{MFPT}_{\Lambda=0}$	1.04 ± 0.08	0.90 ± 0.11	0.57 ± 0.21

quantity like MFPT, we find our effective model useful in distinguishing the underlying differences in terms of the three dynamical modes (Supplemental Material [27]) [40].

Dynamics of an inclusion in a polymeric media is expected to depend on the inclusion size [41]. We find that the effect of TLPA becomes significant for large inclusions (Table I, Supplemental Material [27]) [40].

Our model provides a framework that may be helpful for understanding various active gels [42–45], usually the long-time stochasticity stemming from activity and the short-time modes being thermal. For instance, Refs. [44,45] reported time dependence of inclusion MSDs, which may be related to a reminiscent structural-remodeling-associated mode.

R. D. acknowledges useful discussions he had with Raphaël Voituriez and David Weitz. R. D. and T. H. appreciate Yuting Lou and Akinori Miyamoto for valuable discussions. Authors acknowledge anonymous referees for their insightful comments. This research was supported by Seed fund of Mechanobiology Institute (to J. P., T. H.) and Singapore Ministry of Education Tier 3 grant, MOET32020-0001 (to G. V. S., J. P., T. H.) and JSPS KAKENHI No. JP18H05529 and No. JP21H05759 from MEXT, Japan (to T. S.).

*Corresponding author: rakeshd68@yahoo.com
Present address: Max Planck Institute for the Physics of Complex Systems, Nöthnitzer Strasse 38, 01187 Dresden, Germany.
†Corresponding author: Jacques.Prost@curie.fr
‡Corresponding author: thiraiwa@gate.sinica.edu.tw

[1] Y. S. Mao, B. Zhang, and D. L. Spector, Biogenesis and function of nuclear bodies, Trends Genet. **27**, 295 (2011).
[2] A. Zidovska, The rich inner life of the cell nucleus: Dynamic organization, active flows, and emergent rheology, Biophys. Rev. Lett. **12**, 1093 (2020).
[3] G. V. Shivashankar, *Nuclear Mechanics and Genome Regulation* (Academic Press, Amsterdam, 2010).
[4] A. M. Wood, A. G. Garza-Gongora, and S. T. Kosak, A crowd sourced nucleus: Understanding nuclear organization in terms of dynamically networked protein function, Biochim. Biophys. Acta **1839**, 178 (2014).
[5] L. Zhu and C. P. Brangwynne, Nuclear bodies: The emerging biophysics of nucleoplasmic phases, Curr. Opin. Cell Biol. **34**, 23 (2015).
[6] H. A. Shaban, R. Barth, and K. Bystricky, Navigating the crowd: Visualizing coordination between genome dynamics, structure, and transcription, Genome Biol. **21**, 278 (2020).
[7] E. Soutoglou and T. Misteli, Mobility and immobility of chromatin in transcription and genome stability, Curr. Opin. Genet. Dev. **17**, 435 (2007).
[8] D. M. Suter, Transcription factors and DNA play hide and seek, Trends Cell Biol. **30**, 491 (2020).
[9] B. R. Sabari, Biomolecular condensates and gene activation in development and disease, Dev. Cell **55**, 84 (2020).
[10] J. E. Sleeman and L. Trinkle-Mulcahy, Nuclear bodies: New insights into assembly/dynamics and disease relevance, Curr. Opin. Cell Biol. **28**, 76 (2014).
[11] D. S. W. Lee, N. S. Wingreen, and C. P. Brangwynne, Chromatin mechanics dictates subdiffusion and coarsening dynamics of embedded condensates, Nat. Phys. **17**, 531 (2021).
[12] Y. Zhang, D. S. W. Lee, Y. Meir, C. P. Brangwynne, and N. S. Wingreen, Mechanical frustration of phase separation in the cell nucleus by chromatin, Phys. Rev. Lett. **126**, 258102 (2021).
[13] R. Das, T. Sakaue, G. V. Shivashankar, J. Prost, and T. Hiraiwa, How enzymatic activity is involved in chromatin organization, eLife **11**, e79901 (2022).
[14] L. Baranello, F. Kouzine, and D. Levens, DNA topoisomerases beyond the standard role, Transcription **4**, 232 (2013).
[15] S. H. Chen, N.-L. Chan, and T.-s. Hsieh, New mechanistic and functional insights into DNA topoisomerases, Annu. Rev. Biochem. **82**, 139 (2013).
[16] J. Roca, Topoisomerase II: A fitted mechanism for the chromatin landscape, Nucleic Acids Res. **37**, 721 (2009).
[17] J. L. Nitiss, DNA topoisomerase II and its growing repertoire of biological functions, Nat. Rev. Cancer **9**, 327 (2009).
[18] D. K. Sinha, B. Banerjee, S. Maharana, and G. V. Shivashankar, Probing the dynamic organization of transcription compartments and gene loci within the nucleus of living cells, Biophys. J. **95**, 5432 (2008).
[19] M. Platani, I. Goldberg, A. I. Lamond, and J. R. Swedlow, Cajal body dynamics and association with chromatin are ATP-dependent, Nat. Cell Biol. **4**, 502 (2002).
[20] A. Zidovska, D. A. Weitz, and T. J. Mitchison, Micron-scale coherence in interphase chromatin dynamics, Proc. Natl. Acad. Sci. U.S.A. **110**, 15555 (2013).
[21] D. Saintillan, M. J. Shelley, and A. Zidovska, Extensile motor activity drives coherent motions in a model of interphase chromatin, Proc. Natl. Acad. Sci. U.S.A. **115**, 11442 (2018).
[22] M. Di Pierro, D. A. Potoyan, P. G. Wolynesa, and J. N. Onuchic, Anomalous diffusion, spatial coherence, and viscoelasticity from the energy landscape of human chromosomes, Proc. Natl. Acad. Sci. U.S.A. **115**, 7753 (2018).
[23] G. Shi, L. Liu, C. Hyeon, and D. Thirumalai, Interphase human chromosome exhibits out of equilibrium glassy dynamics, Nat. Commun. **9**, 3161 (2018).
[24] F. M. Hameed, M. Rao, and G. V. Shivashankar, Dynamics of passive and active particles in the cell nucleus, PLoS One **7**, e45843 (2012).
[25] S. M. Görisch, M. Wachsmuth, C. Ittrich, C. P. Bacher, K. Rippe, and P. Lichter, Nuclear body movement is determined by chromatin accessibility and dynamics, Proc. Natl. Acad. Sci. U.S.A. **101**, 13221 (2004).

[26] S. Maharana, D. Sharma, X. Shi, and G. V. Shivashankar, Dynamic organization of transcription compartments is dependent on functional nuclear architecture, Biophys. J. **103**, 851 (2012).
[27] See Supplemental Material at http://link.aps.org/supplemental/10.1103/PhysRevLett.132.058401 for further details about the numerical model, the effective model, and the supporting discussion, which includes Refs. [13,28–32].
[28] A. Jusufi, J. Dzubiella, C. N. Likos, C. von Ferber, and H. Löwen, Effective interactions between star polymers and colloidal particles, J. Phys. Condens. Matter **13**, 6177 (2001).
[29] M. Camargo and C. N. Likos, Phase separation in star-linear polymer mixtures, J. Chem. Phys. **130**, 204904 (2009).
[30] T. Guérin, O. Bénichou, and R. Voituriez, Non-Markovian polymer reaction kinetics, Nat. Chem. **4**, 568 (2012).
[31] T. Guérin, N. Levernier, O. Bénichou, and R. Voituriez, Mean first-passage times of non-Markovian random walkers in confinement, Nature (London) **534**, 356 (2016).
[32] Y. Sakamoto and T. Sakaue, First passage time statistics of non-Markovian random walker: Dynamical response approach, Phys. Rev. Res. **5**, 043148 (2023).
[33] J. E. Lindsley and J. C. Wang, On the coupling between ATP usage and DNA transport by yeast DNA topoisomerase II, J. Biol. Chem. **268**, 8096 (1993).
[34] T. Saito and T. Sakaue, Driven anomalous diffusion: An example from polymer stretching, Phys. Rev. E **92**, 012601 (2015).
[35] A. S. Hansen, A. Amitai, C. Cattoglio, R. Tjian, and X. Darzacq, Guided nuclear exploration increases CTCF target search efficiency, Nat. Chem. Biol. **16**, 257 (2020).
[36] R. Cortini and G. J. Filion, Theoretical principles of transcription factor traffic on folded chromatin, Nat. Commun. **9**, 1740 (2018).
[37] J. H. Lee and J. M. Berger, Cell cycle-dependent control and roles of DNA topoisomerase II, Genes Dev. **10**, 859 (2019).
[38] H. C. Schröder, R. Steffen, R. Wenger, D. Ugarković, and W. E. G. Müller, Age-dependent increase of DNA topoisomerase II activity in quail oviduct; modulation of the nuclear matrix-associated enzyme activity by protein phosphorylation and poly(ADP-ribosyl)ation, Mutat. Res. **219**, 283 (1989).
[39] K. Morotomi-Yano and K. Yano, Nucleolar translocation of human DNA topoisomerase II by ATP depletion and its disruption by the RNA polymerase I inhibitor BMH21, Sci. Rep. **11**, 21533 (2021).
[40] R. Das, T. Sakaue, G. V. Shivashankar, J. Prost, and T. Hiraiwa (to be published).
[41] L.-H. Cai, S. Panyukov, and M. Rubinstein, Mobility of nonsticky nanoparticles in polymer liquids, Macromolecules **44**, 7853 (2011).
[42] T. B. Liverpool, Active gels: Where polymer physics meets cytoskeletal dynamics, Phil. Trans. R. Soc. A **364**, 3335 (2006).
[43] J. Prost, F. Jülicher, and J. F. Joanny, Active gel physics, Nat. Phys. **11**, 111 (2015).
[44] D. Mizuno, C. Tardin, C. F. Schmidt, and F. C. MacKintosh, Nonequilibrium mechanics of active cytoskeletal networks, Science **315**, 370 (2007).
[45] M. Guo, A. J. Ehrlicher, M. H. Jensen, M. Renz, J. R. Moore, R. D. Goldman, J. Lippincott-Schwartz, F. C. Mackintosh, and D. A. Weitz, Probing the stochastic, motor-driven properties of the cytoplasm using force spectrum microscopy, Cell **158**, 822 (2014).